European Journal of Applied Mathematics (2025), 1–25
doi:10.1017/S0956792525000014

CAMBRIDGE UNIVERSITY PRESS

PAPER

Forman–Ricci communicability curvature of graphs and networks

Ernesto Estrada

Institute for Cross-Disciplinary Physics and Complex Systems (IFISC) CSIC-UIB, Palma, de Mallorca, Spain
Email: estrada@ifisc.uib-csic.es

Received: 06 August 2024; **Revised:** 08 January 2025; **Accepted:** 16 January 2025

Keywords: curvature; matrix functions; complex networks; network communicability; communicability distance

2020 Mathematics Subject Classification: 05C50, 53A70 (Primary); 05C21, 53Z99, 51K99 (Secondary)

Abstract

Geometric parameters in general and curvature in particular play a fundamental role in our understanding of the structure and functioning of real-world networks. Here, the discretisation of the Ricci curvature proposed by Forman is adapted to capture the global influence of the network topology on individual edges of a graph. This is implemented mathematically by assigning communicability distances to edges in the Forman–Ricci definition of curvature. We study analytically both the edge communicability curvature and the global graph curvature and give mathematical characterisations of them. The Forman–Ricci communicability curvature is interpreted 'physically' on the basis of a non-conservative diffusion process taking place on the graph. We then solve analytically a toy model that allows us to understand the fundamental differences between edges with positive and negative Forman–Ricci communicability curvature. We complete the work by analysing three examples of applications of this new graph-theoretic invariant on real-world networks: (i) the network of airport flight connections in the USA, (ii) the neuronal network of the worm *Caenorhabditis elegans* and (iii) the collaboration network of authors in computational geometry, where we strengthen the many potentials of this new measure for the analysis of complex systems.

1. Introduction

Graphs $G = (V, E)$ are excellent mathematical objects to represent the networked nature of complex systems [21, 22]. One way of characterising the structure of these networks is by using functions of matrices [40] representing graph structure, e.g., adjacency matrix, Laplacian matrices, shortest-path distance matrix, etc. [7]. In particular, the definition of the so-called network communicability functions [28, 31] has opened many avenues for exploring the relations between network structure and dynamical processes taking place on them [1, 2, 13, 30, 33, 37]. A very attractive characteristic of these functions is that they induce geometric embedding of the graphs into Euclidean spherical spaces [32], allowing the definition of communicability distance functions [20, 23] and angles [29], which can be proved to be connected with non-conservative (NC) diffusive dynamics on the graphs [24] (see references in [24] for the context in which NC diffusion is important). Consequently, communicability geometric functions represent a way to connect graph structure with geometric concepts and dynamical processes taking place on them.

In network geometry [9], where the study of communicability geometry is framed, the concept of curvature [47] plays a fundamental role. Therefore, it has naturally triggered interest for its use to characterise network structure [12]. As a way of characterising the deviation of a geometrical object from being flat, the concept of curvature has found many applications in network theory in a variety of real-world scenarios [6, 11, 18, 19, 35, 45, 49, 51–53, 55, 58, 60]. There have been several approaches to

characterise the discrete curvature in graphs, such as the Gromov-hyperbolic curvature [12, 39, 41], the combinatorial curvature [18, 48], discretizations of Ricci curvature [8, 56], such as the Ollivier–Ricci curvature [50], the Bakry–Émery Ricci curvature [3] and the Forman–Ricci curvature [34], as well as ad hoc network curvatures [15, 16] which are related to discretizations of Ricci curvature. The three discrete Ricci curvatures previously mentioned have been compared [51] for the analysis of biological networks where they were shown to yield similar results. However, Forman–Ricci curvature has been pointed out by several authors as having some advantages over the others. For instance, it can be defined on directed positively weighted networks [51]. It does not require such intensive calculations like the Ollivier–Ricci curvature, which necessitates solving a linear programming problem [55], and it is naturally related to edges, which are the discrete analogue of a vector in a graph/network. Also, the fact that the Forman–Ricci curvature (see next section) is defined using weights for edges allows the use of edge invariants based on communicability functions, such as communicability distance, to characterise the influence of the global topology of a network on the curvature of an edge. The use of other distances, such as the resistance distance [42], is also appropriate in this context. It has been implemented in some ad hoc curvature measures, such as in refs. [15, 16]. However, contrary to what happen with the communicability distance, the resistance distance and the shortest path distance are identical for trees. This makes that the Forman–Ricci curvature based on resistance distance for trees depends only on the degree of the corresponding edge (see further in this work), removing any influence of the global topology of the graph on its curvature. It has also been proved that the resistance distance is useless for network navigability in relatively large graphs [57], which also adds a negative point on its use for network analysis.

Here, we consider the Forman–Ricci curvature of a graph in which every edge is characterised by its communicability distance. In this way, every edge 'feels' the influence of the global topology of the graph. We first define the edge Forman–Ricci communicability curvature and give some characterisation of it. We then define the global Forman–Ricci communicability curvature as the sum of edge curvatures and give a structural and physical interpretation of its meaning. We build a toy model which we solve analytically allowing us to understand the fundamental differences between edges with positive and negative communicability curvature. Additionally, we provide analytical and computational evidence about the meaning of the positive/negative global curvature of graphs on the basis of NC diffusive dynamics taking place on the graph. Finally, we provide three examples of applications of this new graph invariant on real-world networks: (i) the network of airport flight connections in the USA, (ii) the neuronal network of the worm *C. elegans* and (iii) the collaboration network of authors in computational geometry.

2. Preliminaries

Here, we consider undirected graphs $G = (V, E)$ with set of vertices $V = \{v_1, \ldots, v_n\}$ and set of edges $E = \{e_1, \ldots, e_m\}$. The adjacency matrix of the graph is designated by A with entries A_{ij} equal to the weight of the corresponding edge or zero otherwise. The degree of a vertex v is the sum of the weights of edges incident to it and is designated by k_v. Except if we say otherwise, we will mainly consider unweighted graphs, i.e., $A_{i,j} = 1$ if $(i, j) \in E$ or zero otherwise. The following standard graph theoretic notation is used: P_n for path graph on n vertices – a graph with all vertices of degree two but two vertices of degree one; C_n for cycle graph on n vertices – the graph with every vertex of degree two and K_n for complete graph on n vertices – the graph with every pair of vertices connected. A complete bipartite graph K_{n_1,n_2} is a graph formed by two disjoint sets of vertices $V_1 \cup V_2$ of n_1 and n_2 vertices, respectively, such that every vertex in V_1 is connected to every vertex in V_2 and vice versa. The star graph is the complete bipartite graph $K_{n-1,1}$. A hypercube graph Q_n is the graph formed from the vertices and edges of an n-dimensional hypercube.

A walk of length k is a sequence of (not necessarily different) vertices $x_1, x_2, \ldots, x_k, x_{k+1}$ such that for each $i = 1, 2, \ldots, k$ there is an edge from x_i to x_{i+1}. The walk is closed if $x_{k+1} = x_1$. A path between two vertices is a walk without repetition neither of vertices nor of edges. A closed path is a cycle.

https://doi.org/10.1017/S0956792525000014 Published online by Cambridge University Press

The number of walks of length k between vertices v and w is given by $\left(A^k\right)_{vw}$. Then, we have the following [28, 31].

Definition 1. *Let $G=(V,E)$ be a graph and let $v,w\in V$ be two vertices (not necessarily adjacent). Then, the communicability function between the two vertices counts the total number of walks between them by giving more weight to the shorter than to the longer ones by means of a factorial penalisation:*

$$\Gamma_{v,w}(G) := \sum_{k=0}^{\infty} \frac{\left(A^k\right)_{vw}}{k!} = \left(e^A\right)_{vw}, \tag{1}$$

where e^A is the matrix exponential of A (see [40] for matrix functions).

The term $\Gamma_{v,v}(G)$ is also known as the subgraph centrality [31] of the vertex v and accounts for the total number of weighted walks that starts and ends at the same vertex. That is, it accounts for the number of a sort of dead ends walks. The term $\Gamma_{v,w}(G)$ for $v\neq w$ accounts for the communicable routes between the two vertices. Therefore, the following quantity has been defined [20].

Definition 2. *Let v and w be two distinct vertices of the graph G. Let*

$$\xi_{v,w} := \Gamma_{v,v}(G) + \Gamma_{w,w}(G) - 2\Gamma_{v,w}(G). \tag{2}$$

Theorem 3. *[20] Let Λ be the diagonal matrix of eigenvalues of A and let V be the matrix whose columns are its orthonormalised eigenvectors. Then, the quantity $\xi_{v,w}$ is a squared Euclidean distance between the vertices v and w of G, which can be written as*

$$\xi_{v,w} = \|x_v - x_w\|^2, \tag{3}$$

where $x_v := e^{\Lambda/2}\varphi_v$ is the position vector of the vertex v in the Euclidean space and φ_v is the vth row of V.

Therefore, the term $\tilde{\xi}_{v,w} := \sqrt{\xi_{v,w}}$ is called the communicability distance between the pairs of vertices v and w of the graph.

The communicability function can be generalised to $\Gamma_{v,w}(G,\beta) := \left(e^{\beta A}\right)_{vw}$ where $\beta\in\mathbb{R}$ [27] is a parameter and so $\xi_{v,w}(\beta) := \Gamma_{v,v}(G,\beta) + \Gamma_{w,w}(G,\beta) - 2\Gamma_{v,w}(G,\beta)$ is the squared communicability distance. Let $D(\beta)\in\mathbb{R}^{n\times n}$ be the matrix whose non-diagonal entries are $\xi_{v,w}(\beta)$ and zero otherwise. Then, $D(\beta)$ is called a Euclidean distance matrix, and the vertices of the graph represent points $p^1,p^2,\ldots,p^n$ in some Euclidean space $\mathbb{R}^r$ [4, 17, 38, 43].

The communicability function and the geometry induced by it are related to some parameters of diffusive dynamics taking place on the graph. Therefore, we will introduce here the basic concepts of such dynamics to be used in this work. Let $C(t)\in\mathbb{R}^{n\times 1}$ be a vector of concentrations of items at the vertices of G at the time t, and let the entries of $\dot{C}(t)$ be the change of these concentrations in time, i.e., $\dot{C}_i(t) = dC_i(t)/dt$, according to a diffusive process of the type: $\dot{C}(t) = -LC(t)$, with initial condition $C(0)=C^0$, where the graph Laplacian operator is $L=K-A$, where K is the diagonal matrix of vertex degrees and A is the adjacency matrix of the graph [24]. The solution of the diffusion equation is $C(t) = \exp(-tL)C^0$. Let us take the sum of the entries of $C(t)$ at an arbitrary time t, $\mathbf{1}^TC(t) = \mathbf{1}^Te^{-tL}C^0$, and expand it using the Taylor series:

$$\mathbf{1}^TC(t) = \mathbf{1}^TC^0 - t\mathbf{1}^TLC^0 + \frac{t^2}{2!}\mathbf{1}^TL^2C^0 + \cdots + \left(\frac{(-1)^k t^k}{k!}\right)\mathbf{1}^TL^kC^0 + \cdots. \tag{4}$$

Then, because L is positive semidefinite, we have that $\mathbf{1}^TL=0$ and so $\left(\mathbf{1}^TL\right)L^{k-1}=0$, so that $\mathbf{1}^TC(t) = \mathbf{1}^TC^0$ for any t. This means that the total concentration of items is conserved at the vertices of the graph in time. We call this process a conservative diffusion.

Let us now replace the standard graph Laplacian L by the Lerman–Ghosh Laplacian $\mathscr{L}_\chi := \chi I - A$, which was first analysed in [36, 44]. Let us then consider the following diffusive process

$$\dot{C}(t) = -(\chi I - A)C(t) = -\mathscr{L}_\chi C(t), \tag{5}$$

https://doi.org/10.1017/S0956792525000014 Published online by Cambridge University Press

with initial condition $C(0) = C^0$. The solution of (5) is given by

$$C(t) = e^{-t(\chi I - A)} C^0. \tag{6}$$

Obviously, the communicability function is exactly the concentration $C(t)$ when $\chi = 0$ and $t = 1$. Other connections will be evident across this paper.

Theorem 4. *[24] Let G be a simple graph and let λ_1 be the spectral radius of its adjacency matrix. Let ψ_1 be the normalised eigenvector corresponding to λ_1. Then, the solution of the diffusion model (5) is given by*

$$\lim_{t\to\infty} C(t) = \begin{cases} \left(\psi_1^T C^0\right)\psi_1 e^{t(\lambda_1-\chi)} = \infty \text{ for } \chi < \lambda_1 \\ \left(\sum_j C_j^0 \psi_1(j)\right)\psi_1 \text{ for } \chi = \lambda_1 \\ \left(\psi_1^T C^0\right)\psi_1 e^{-t(\chi-\lambda_1)} = 0 \text{ for } \chi > \lambda_1. \end{cases} \tag{7}$$

Therefore, the concentration of items at the vertices of G is not conserved in time, i.e., it may diverge if $\chi < \lambda_1$, vanish if $\chi > \lambda_1$, or reach a steady state with sum of concentrations smaller than the ones in C^0 if $\chi = \lambda_1$. If G is a regular graph, then, the diffusion model (5) with $\chi = \lambda_1$ is conservative for any initial condition, where $\lim_{t\to\infty} C_i(t) = \frac{1}{n}\sum_j C_j^0$ for all $j \in V$. If the graph is not regular and $C^0 \neq \psi_1$ then the process is NC and $0 < C(t) < C^0 < \infty$. Thus, we call this process the NC diffusion model on the graph.

3. Definition of edge communicability curvature

Let us start by introducing the definition of the Forman–Ricci curvature of an edge in a graph (for details see [34]).

Definition 5. *The Forman–Ricci curvature of an edge $e = (v, w) \in E$ is defined by*

$$F_e := w_e\left(\frac{w_v}{w_e} + \frac{w_w}{w_e} - \sum_{e_l\sim v}\frac{w_v}{\sqrt{w_e w_{e_l}}} - \sum_{e_l\sim w}\frac{w_w}{\sqrt{w_e w_{e_l}}}\right), \tag{8}$$

where w_v, w_w and w_e are the weights of vertices v and w, and of edge e. The sums over $e_l \sim k$ run over all edges e_l incident on the vertex k excluding e, and in case the vertex has degree one, this term is taken to be zero.

Remark 6. Let G be an unweighted graph, i.e., $w_v = w_w = w_e = 1$. Then,

$$F_e := 2 - (k_v - 1) - (k_w - 1) = 4 - k_v - k_w, \tag{9}$$

which will be called here the unweighted Forman–Ricci curvature.

In this definition, an edge e of the graph could be weighted by any $w_e \in \mathbb{R}$. Therefore, a natural way of proceeding is to consider that every edge of the graph is weighted by its communicability distance. We introduce this formulation here in a formal way.

Let us consider every edge $e = vw$ in E as a compact one-dimensional manifold with boundary $\partial e = v \cup w$. Let the edge $e = vw$ be given the metric $\mathbb{L}_{vw}$, such that [10, 46]

$$\tilde{e}_{vw} \underset{isom}{\cong} \begin{bmatrix} [0, \xi_{vw}] & (v, w) \in E \\ 0 & (v, w) \notin E \end{bmatrix}. \tag{10}$$

We then extend the distance metric $\mathbb{L}_{vw}$ on the edges of G via infima of lengths of curves in the geometrisation of G [10, 46]. This can be practically implemented as follows.

Definition 7. *Let $D(\beta)$ be the square, symmetric matrix whose v, w entries are $\xi_{vw}(\beta)$. Then, $W(\beta) := A \odot D(\beta) = D(\beta) \odot A$ is the weighted adjacency matrix of G, where every edge receives a weight equal*

https://doi.org/10.1017/S0956792525000014 Published online by Cambridge University Press

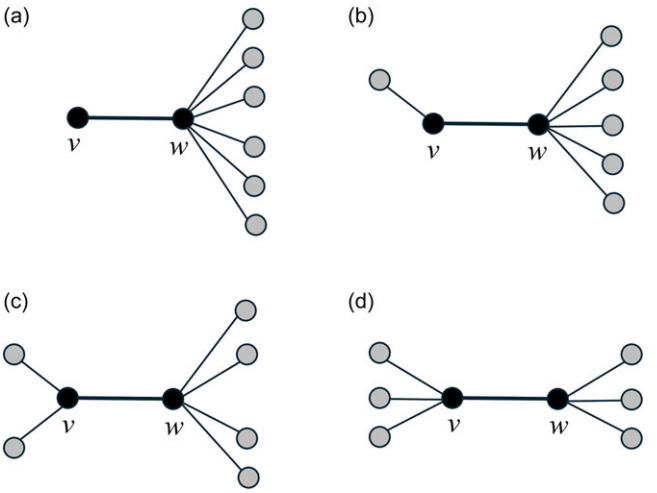

Figure 1. *Illustration of four trees for which we report the values of the edge curvature for the edge marked by the two black vertices.*

to the communicability distance between the pair of vertices forming the edge. Here, $\odot$ is the Hadamard product (also Schur or entrywise product) of two matrices defined for any two matrices $P \odot Q$ as the matrix with entries $(P \odot Q)_{ij} = (P)_{ij} (Q)_{ij}$.

Definition 8. *Let $\tilde{G}(\beta)$ be the weighted graph whose adjacency matrix is given by $W(\beta)$. Then, the communicability Forman–Ricci curvature of an edge $e = (v, w) \in E$ in $\tilde{G}(\beta)$ is given by*

$$\mathcal{C}_{e=v,w}(G, \beta) := 2 - \sum_{k \sim v} \sqrt{\frac{\xi_{vw}(\beta)}{\xi_{vk}(\beta)}} - \sum_{k \sim w} \sqrt{\frac{\xi_{vw}(\beta)}{\xi_{wk}(\beta)}}, \tag{11}$$

where $k \neq v, w$, and where the first sum is carried out for all edges which are incident to the vertex v and the second sum is for all edges incident to the vertex w. If such edge does not exist, the term is taken to be zero.

Example 9. *Let us consider the trees illustrated in Figure 1. We selected these trees because of the following reasons. The first is that the edge $(v, w) \in E$ marked in black in the graphs has the same edge degree $(k_v + k_w - 2)$; therefore, they have the same unweighted Forman–Ricci curvature. Because the resistance distance and the shortest path distances coincide for trees, the resistance curvature [15] for these edges is exactly the same for this edge in the four trees. However, the edges are surrounded by very different topological environments in those trees.*

In Table 1, we give the values of $\mathcal{C}_{(v,w)}$ using $\beta = 1$ for the marked edge in the four trees of Figure 1. As can be seen, the communicability curvature changes systematically from graph a) to d) indicating the influence of the global topology on the otherwise locally equivalent edges.

We then have the following result.

Lemma 10. *Let $F_{e=v,w}(G)$ be the unweighted Forman–Ricci curvature edge $(v, w) \in E$ in the simple graph G, and let $\mathcal{C}_{e=v,w}(G, \beta)$ be the Forman–Ricci communicability curvature of the same edge. Then,*

$$\lim_{\beta \to 0} \mathcal{C}_{e=v,w}(G, \beta) = F_{e=v,w}(G). \tag{12}$$

https://doi.org/10.1017/S0956792525000014 Published online by Cambridge University Press

Table 1. *Values of the communicability curvature for the four trees in Figure 1. The edge v, w has the same unweighted Forman–Ricci curvature as well as the same resistance distance curvature [15] in the four graphs, which are equal to -4. All the calculations were performed by using $\beta = 1$*

graph	$\mathcal{C}_{(v,w)}$
a	-4
b	-4.7642
c	-5.0955
d	-5.1839

Proof. Let us define $s(\beta) := diag\left(e^{\beta A}\right)$ as the column vector formed by the main diagonal entries of $e^{\beta A}$. Then,

$$D(\beta) = s(\beta)\,\mathbf{1}^T + \mathbf{1}s(\beta)^T - 2e^{\beta A}. \tag{13}$$

Then, $\lim_{\beta\to 0} e^{\beta A} = Id$ where Id is the identity matrix. Therefore, $\lim_{\beta\to 0} D(\beta) = 2(J - Id)$, where $J = \mathbf{1}\mathbf{1}^T$ is an all-ones matrix and $\lim_{\beta\to 0} \mathcal{C}_{e=v,w}(G,\beta) = 4 - k_v - k_w$, which proves the result. □

Remark 11. If we interpret $\beta = (kT)^{-1}$ (see [27]) as the inverse temperature of a thermal bath in which the graph is submerged to, then, the unweighted Forman–Ricci curvature represents the Forman–Ricci communicability curvature when the temperature goes to infinity, which is an extreme case where the structure of the graph beyond the nearest neighbours of the vertices is not taken into account.

Lemma 12. *Let P_n be the path graph with n vertices labelled in increasing order from one of its pendant vertices. Then, for any $\beta \in \mathbb{R}$,*

$$\mathcal{C}_{1,2}(P_n, \beta) > 0. \tag{14}$$

Proof. As we have proved before in this case $\mathcal{C}(P_n, \beta) = F(P_n) = 2$, which is positive. Then, let us focus on $\beta \neq 0$. Let us label the vertices of P_n in consecutive order from one of the pendant vertices. Let $i \leq n/2$ (n even) or $i \leq (n+1)/2$ (n odd) be any vertex of P_n, then the communicability distance of the edge $(i, i+1) \in E$ for sufficiently large n is given by [20]

$$\xi_{i,i+1}(\beta) = 2I_0(2\beta) - 2I_1(2\beta) - I_{2i}(2\beta) - I_{2(i+1)}(2\beta) + 2I_{2i+1}(2\beta), \tag{15}$$

where

$$I_\nu(z) := \frac{1}{\pi}\int_0^\pi e^{z\cos\theta}\cos(\nu\theta)\,d\theta, \tag{16}$$

is the modified Bessel function of the first kind. Let

$$\mathcal{C}_{1,2}(P_n, \beta) = 2 - \sqrt{\frac{\xi_{1,2}(\beta)}{\xi_{2,3}(\beta)}} \tag{17}$$

We now prove that

$$\sqrt{\frac{\xi_{1,2}(\beta)}{\xi_{2,3}(\beta)}} < 2. \tag{18}$$

https://doi.org/10.1017/S0956792525000014 Published online by Cambridge University Press

For it, we write

$$\sqrt{\frac{2I_0(2\beta)-2I_1(2\beta)-I_4(2\beta)-I_2(2\beta)+2I_3(2\beta)}{2I_0(2\beta)-2I_1(2\beta)-I_4(2\beta)-I_6(2\beta)+2I_5(2\beta)}} \overset{?}{<} 2, \tag{19}$$

so that

$$2I_0(2\beta)-2I_1(2\beta)-I_4(2\beta) \overset{?}{>} 2I_3(2\beta)-I_2(2\beta)-8I_5(2\beta)+4I_6(2\beta), \tag{20}$$

which is arranged to

$$2I_0(2\beta)+I_2(2\beta)+8I_5(2\beta) \overset{?}{>} 2I_1(2\beta)+2I_3(2\beta)+I_4(2\beta)+4I_6(2\beta). \tag{21}$$

Using the recursive formula for the modified Bessel function of the first kind: $I_{r+1}(z)=I_{r-1}(z)-\frac{2}{z}I_r(z)$, we have

$$2I_0(2\beta)+\frac{3}{\beta}I_3(2\beta)+8I_5(2\beta) \overset{?}{>} 2I_1(2\beta)+2I_3(2\beta)+4I_6(2\beta). \tag{22}$$

Because $I_0(2\beta)>I_1(2\beta)$ and $8I_5(2\beta)>4I_6(2\beta)$ we have that, for any $\beta<3/2$, $\frac{3}{\beta}I_3(2\beta)>2I_3(2\beta)$, such that the previous inequality is true. Let us now consider the case $\beta>3/2$ and prove whether

$$\frac{3}{\beta}I_3(2\beta)+8I_5(2\beta) \overset{?}{>} 2I_3(2\beta)+4I_6(2\beta). \tag{23}$$

We rewrite it as

$$\left(\frac{3}{\beta}-2\right)I_3(2\beta) \overset{?}{>} 4I_6(2\beta)-8I_5(2\beta), \tag{24}$$

so that we have

$$\left(\frac{3}{\beta}-2\right)I_3(2\beta)>0>4\left(I_6(2\beta)-I_5(2\beta)\right)-4I_5(2\beta), \tag{25}$$

which proves that $\mathcal{C}_{1,2}(P_n,\beta)>0$ for any $\beta\in\mathbb{R}$. □

Definition 13. *Two edges e_1 and e_2 are automorphically equivalent if there is a permutation of the two edges that leave the adjacency matrix of G unaltered. That is, if P is the permutation matrix corresponding to a permutation π of the vertex set of a graph G, and A is the adjacency matrix of the graph, then π is an automorphism of G iff $PAP^T=A$. The orbit of an edge d is the set of all edges $e\in E$ in the graph $G=(V,E)$ such that there is an automorphism ϕ such that $\phi(d)=e$. The graph in which all the edges are in the same orbit is known as edge-transitive graph.*

Lemma 14. *Let G be an edge graph in which every pair of vertices are automorphically equivalent. Then,*

$$\mathcal{C}_{i,j}(G,\beta)=F_{i,j}(G), \tag{26}$$

Proof. Two edges which are automorphically equivalent have the same communicability distance. Therefore, in the edge-transitive graph, all edges have the same communicability distance, i.e., $\xi_{wk}(\beta)=\xi_{vw}(\beta)$ for every edge $(w,k)\in E$. Consequently, $\sum_{k\sim v}\sqrt{\frac{\xi_{vw}(\beta)}{\xi_{vk}(\beta)}}=k_v-1$ and so $\mathcal{C}_e(G,\beta)=4-k_v-k_w=:F_e(G)$. □

Corollary 15. *Let C_n, Q_d, K_{n_1,n_2}, and K_n be the cycle graph on n vertices, the hypercube graph of dimension d, the complete bipartite with partition $V_1\cup V_2=V$ and $\#V_1=n_1, \#V_2=n_2$ and the complete graph*

https://doi.org/10.1017/S0956792525000014 Published online by Cambridge University Press

on n vertices, respectively. Let $(i,j) \in E$ be any edge in each of these graphs. Then,

$$\mathcal{C}_{i,j}(G,\beta) = F_{i,j}(G) = \begin{cases} 0 & G = C_n \\ 4-2d & G = Q_d \\ 4-n_1-n_2 & G = K_{n_1,n_2} \\ 2(3-n) & G = K_n. \end{cases} \tag{27}$$

3.1 What is the meaning of the communicability curvature?

To understand the meaning of the communicability curvature of an edge, we will start by considering the NC diffusion dynamics described in Preliminaries (see also [24]). For the sake of simplicity, let us consider the case $\chi = 0$ in $\mathscr{L}_\chi := \chi I - A$, such that $\mathscr{L}_\chi = -A$, (for $\chi \neq 0$ the results are qualitatively the same), and let us focus on a couple of vertices designated by v and w. At the local level, the concentration of items at a vertex i at time t is given by

$$\dot{C}_i(t) = \left(\sum_{(i,j)\in E} C_j(t) \right), \tag{28}$$

because $-\chi C_i(t) = 0$. The solution of the NC diffusion model can be written as

$$C(t) = e^{t(\lambda_1-\chi)} \left(\psi_1^T C^0\right) \psi_1 + e^{t(\lambda_2-\chi)} \left(\psi_2^T C^0\right) \psi_2 + \cdots + e^{t(\lambda_n-\chi)} \left(\psi_n^T C^0\right) \psi_n, \tag{29}$$

where $\lambda_1 > \lambda_2 \geq \ldots \geq \lambda_n$ are the eigenvalues of A and ψ_j is the normalised eigenvector corresponding to λ_j.

Then, at a given time, the concentration at these nodes are

$$C_v(t) = \sum_j \left(\exp(tA)\right)_{vj} C_j^0 \tag{30}$$

and

$$C_w(t) = \sum_j \left(\exp(tA)\right)_{wj} C_j^0. \tag{31}$$

Then, let us define

$$\mathscr{E}_{vw|C_j^0=\delta_{jv}} = C_{v|C_j^0=\delta_{jv}}(t) - C_{w|C_j^0=\delta_{jv}}(t). \tag{32}$$

As we have placed all the concentration at vertex v at the initial time, i.e., $C_{v|C_j^0=\delta_{jv}}(t=0) = 1$, at $t=0$, there is no concentration at w and the difference $\mathscr{E}_{vw|C_j^0=\delta_{jv}}$ is maximum. As the time passes, the concentration $C_{w|C_j^0=\delta_{jv}}(t)$ increases, while that at v drops, making $\mathscr{E}_{vw|C_j^0=\delta_{jv}}$ smaller. At the equilibrium, we expect that $C_{v|C_j^0=\delta_{jv}}(t) = C_{w|C_j^0=\delta_{jv}}(t)$, such that the term $\mathscr{E}_{vw|C_j^0=\delta_{jv}}$ reaches its minimum value, which is zero. Therefore, we claim that $\mathscr{E}_{vw|C_j^0=\delta_{jv}}$ quantifies the *distance from equilibrium* (DFE) for the pair of vertices v to w in a graph when the initial concentration is totally located at the vertex v, $C_0(j) = \delta_{j,v}$, where $\delta_{i,j}$ is the Kronecker delta. Let us define the same in the other direction when the initial concentration is completely located at the vertex w,

$$\mathscr{E}_{wv|C_j^0=\delta_{jw}} = C_{w|C^0=\delta_{jw}}(t) - C_{v|C_j^0=\delta_{jw}}(t). \tag{33}$$

Let us now define the sum of the DFE between the two nodes in both directions, which is given by

$$\mathscr{E}_{vw|C_j^0=\delta_{jv}} + \mathscr{E}_{wv|C_j^0=\delta_{jw}} = \left(\exp(tA)\right)_{vv} + \left(\exp(tA)\right)_{ww} - 2\left(\exp(tA)\right)_{vw}, \tag{34}$$

https://doi.org/10.1017/S0956792525000014 Published online by Cambridge University Press

which obviously is the squared communicability distance between v and w when $t = \beta$. Therefore, the Forman–Ricci communicability curvature of the edge $(v, w) \in E$ can be expressed as

$$\mathcal{C}_{v,w}(G,\beta) = 2 - \sum_{k\sim v} \sqrt{\frac{\mathcal{E}_{vw}|_{C_j^0=\delta_{jv}} + \mathcal{E}_{wv}|_{C_j^0=\delta_{jw}}}{\mathcal{E}_{vk}|_{C_j^0=\delta_{jv}} + \mathcal{E}_{kv}|_{C_j^0=\delta_{jk}}}} - \sum_{k\sim w} \sqrt{\frac{\mathcal{E}_{vw}|_{C_j^0=\delta_{jv}} + \mathcal{E}_{wv}|_{C_j^0=\delta_{jw}}}{\mathcal{E}_{wk}|_{C_j^0=\delta_{jw}} + \mathcal{E}_{kw}|_{C_j^0=\delta_{jk}}}}. \tag{35}$$

Notice that by taking the square roots of $\xi_{i,j}(G,\beta)$, we are directly considering the communicability distances, not their squares. The first summation represents the ratio of the DFE between the vertices v and w relative to the DFE between the vertex v and its nearest neighbours. That is, if the pair of vertices v and w reaches an equilibrium of concentrations faster than v and its nearest neighbours, then this term is smaller than one because the DFE for v and w is smaller than that between v and its nearest neighbours. The second summation is the same for the DFE between v and w and the one between w and its nearest neighbours. Therefore, if the edge formed by v and w reaches an equilibrium in a faster way that the edges conforming the nearest neighbours of v and of w, i.e., if DFE of v, w is smaller than that of the nearest neighbours of both vertices, then $\mathcal{C}_{v,w}(G,\beta) > 0$. However, if the pair v, w displays larger DFE that their nearest neighbours, then $\mathcal{C}_{v,w}(G,\beta) < 0$. Let us illustrate this by an example.

Example 16. *Let us consider the three graphs illustrated in Figure 2 in which we will focus on the curvature of the edge* (i,j)*. The three graphs are cycle graphs of 4 vertices in which one edge has weights equal to 1 (a), 2 (b) and 1/2 (c). We computed the curvature of the three edges in question which are given in Table 2. As can be seen the curvature of the edge* (i,j) *in a) is zero, in b) is positive and in c) is negative. From our previous interpretation, we have that in a) the edge* (i,j) *has DFE identical to those of the nearest neighbours of i and j, respectively, which is obvious by the symmetry of this graph. In b) the edge* (i,j) *has significantly smaller DFE than* (i,l) *and* (j,k)*. This means that a concentration of items placed at i (resp. at j) will reach an equilibrium with j (resp. with i) in a much faster way than with l (resp. with k). The reason is obvious from the fact that there is a double number of ''lanes'' of communication between i and j, than between them and their respective nearest neighbours. Finally, the case c) shows that* (i,j) *has more ''difficulties'' to reach the equilibrium than their nearest neighbours also by obvious reasons.*

To check about the meaning of these results, we use the NC diffusion dynamics (5) by using $\chi = \lambda_1(G)$ where $\lambda_1(G)$ is the spectral radius of the adjacency matrix of the corresponding graph. We use this value of χ because, although the process is NC, it has a steady state and we can measure $t_c(i)$ and $t_c(j)$, which are the times at which $|C_i(t_c) - C_i(t_c - 1)| \leq 10^{-3}$ and $\left|C_j(t_c) - C_j(t_c - 1)\right| \leq 10^{-3}$, respectively, both with initial condition $C_r^0 = \delta_{ri}$. Then, in Table 2, we report $t_c(i,j) = (t_c(i) + t_c(j))/2$, which is the average time at which the edge under analysis reaches the steady state when the particles are placed at one of its endpoints. We can see that the edge i, j of positive curvature (graph b) reaches the steady state in a shorter time than the one of zero curvature (graph a), and that the edge with negative curvature (graph c) reaches the steady state in a longer time. The fact that the edge with positive curvature reaches the steady state faster than the one of zero curvature is a signature of the high communicability between i and j in the graph b), i.e., every time that information reaches j, it is immediately transferred back to i. In graph c), both vertices i and j reach their steady states at much longer times that in graph a) due to the fact that the low communicability between i and j compromises the interchange of information between them, delaying the consensus.

We can build an analogy between the edges with negative and positive curvature with the set of arteries and capillaries in the human body. Arteries interconnects different organs in the body. Therefore, as organs are highly interconnected among them, they have large degrees, and the curvature of these arteries is expected to be negative. Continuing with the analogy, capillaries resemble those edges with positive curvature, which interconnects different regions inside the same organ. We can then use the metaphor of considering edges of negative curvature as arteries in the graphs and those of positive curvature as capillaries.

https://doi.org/10.1017/S0956792525000014 Published online by Cambridge University Press

Table 2. *Values of the communicability curvature of the edge i,j using $\beta = 1$ in the three graphs illustrated in Figure 2 as well as the average time at which the edge under analysis reaches the steady state when the particle is placed at one of its vertices relative to the graph a)*

	$\mathcal{C}_{i,j}(G)$	$t_c(i,j)$
a	0	1.000
b	1.0665	0.978
c	−0.6390	1.652

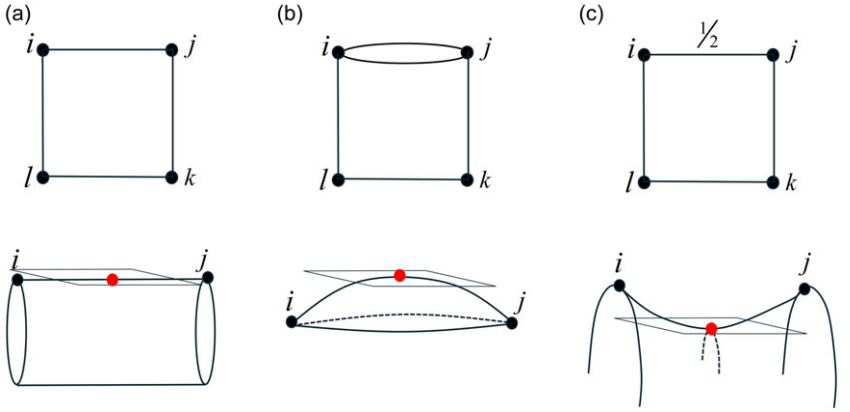

Figure 2. *Illustration of three graphs formed by a four-vertices cycle in which the edge i,j is weighted by 2 in graph (b) and by 1/2 in graph (c). In the bottom line, we draw a pictorial representation of what the curvature of the i,j edge means. All the calculations are performed using $\beta = 1$.*

3.1.1 A model of arteries and capillaries

Let us consider two classes of graphs, namely the wheel graph on n vertices W_n ($n \geq 4$) and the friendship graph F_n ($n \geq 5$). A wheel graph W_n is the graph consisting of a cycle C_{n-1} in which every vertex is connected to a central vertex i as illustrated in the Figure 3(a). The friendship graph consists of $(n-1)/2$ triangles which are glued to a common vertex as illustrated in Figure 3(b). Both graphs can be seen as a core formed by the vertex i and a periphery formed by the rest of vertices. We can consider that the friendship graph is constructed from the wheel one by removing alternant edges of the cycle when the number of vertices is odd. Therefore, while in the wheel, there is a cycle which connects all the vertices in the periphery. This cycle is interrupted in the friendship graph and the circulation across the periphery is impeded, such that most circulation, except that between pairs forming the same triangle, needs to be taken across the central vertex i (see Figure 3).

It is easy to realise that the curvature for $\beta = 1$ of the edge $(i,j) \in E$ in both graphs is negative

$$\mathcal{C}_{ij}(W_n) = (1-n) - 2\sqrt{\frac{\xi_{ij}(W_n)}{\xi_{jj'}(W_n)}} < 0, \tag{36}$$

$$\mathcal{C}_{ij}(F_n) = (1-n) - \sqrt{\frac{\xi_{ij}(F_n)}{\xi_{jj'}(F_n)}} < 0. \tag{37}$$

https://doi.org/10.1017/S0956792525000014 Published online by Cambridge University Press

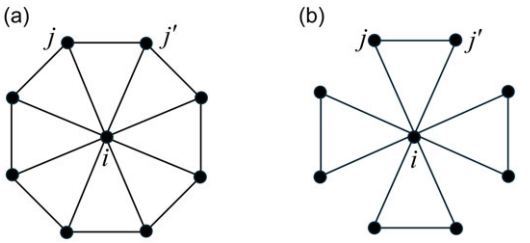

Figure 3. *Illustration of a wheel (a) and friendship (b) graphs with nine vertices and the distinct vertices labelled by i for the central vertex and j, j′ for a peripheric edge.*

Therefore, let us then focus on the curvature of the edge $(j, j') \in E$ in both graphs.

Theorem 17. *Let $(j, j') \in E$ be an edge between two peripheric vertices in W_n. Then, for $\beta = 1$*

$$\mathcal{C}_{jj'}(W_n) = -2\sqrt{\frac{\xi_{jj'}(W_n)}{\xi_{ij}(W_n)}} < 0, \tag{38}$$

and let $(j, j') \in E$ be an edge between two peripheric vertices in F_n and let $t = \sqrt{4n-3}$. Then,

$$\mathcal{C}_{jj'}(F_n) = 2\left(1 - \sqrt{\frac{\xi_{jj'}(F_n)}{\xi_{ij}(F_n)}}\right), \tag{39}$$

where

$$\xi_{jj'}(F_n) = \frac{2}{e}, \tag{40}$$

and

$$\xi_{ij}(F_n) = \frac{n(t-1)+2}{2t(n-1)} e^{\frac{1+t}{2}} + \frac{n(t+1)-2}{2t(n-1)} e^{\frac{1-t}{2}} + \frac{e^2 n + n - 3e^2 - 1}{2e(n-1)} - \frac{4\sqrt{e}}{t} \sinh\frac{t}{2}, \tag{41}$$

which means that $\mathcal{C}_{jj'}(F_n) > 0$.

Proof. It is easy to see that

$$\mathcal{C}_{jj'}(W_n) = 2 - 2\sqrt{\frac{\xi_{jj'}(W_n)}{\xi_{ij'}(W_n)}} - 2\sqrt{\frac{\xi_{jj'}(W_n)}{\xi_{ij}(W_n)}} = -2\sqrt{\frac{\xi_{jj'}(W_n)}{\xi_{ij}(W_n)}}. \tag{42}$$

Let us then focus on obtaining $\xi_{ij}(F_n)$ and $\xi_{jj'}(F_n)$. First, we obtain the eigenvalues and eigenvectors of F_n:

$$\lambda_j = \left\{ \frac{1+t}{2}, 1^{\left(\frac{n-3}{2}\right)}, -1^{\left(\frac{n-1}{2}\right)}, \frac{1-t}{2} \right\}, \tag{43}$$

where the superindices represent the multiplicity of the eigenvectors, and $\psi_1(i) = \sqrt{\frac{t-1}{2t}}$, $\psi_1(j) = \sqrt{\frac{2}{t^2-t}}$, $\psi_n(i) = \sqrt{\frac{t+1}{2t}}$, $\psi_1(j) = \sqrt{\frac{2}{t^2+t}}$, such that we can get

$$\left(e^{A(F_n)}\right)_{ii} = \left(\frac{t-1}{2t}\right) e^{\frac{t+1}{2}} + \left(\frac{t+1}{2t}\right) e^{\frac{1-t}{2}}, \tag{44}$$

https://doi.org/10.1017/S0956792525000014 Published online by Cambridge University Press

and

$$\left(e^{A(F_n)}\right)_{jj} = \frac{tr\left(e^{A(F_n)}\right) - \left(e^{A(F_n)}\right)_{ii}}{n-1}, \tag{45}$$

where $tr\left(e^{A(F_n)}\right) = \sum_{j=1}^{n} e^{\lambda_j(F_n)}$,

$$tr\left(e^{A(F_n)}\right) = e^{\frac{t+1}{2}} + e^{\frac{1-t}{2}} + \frac{e^2 n + n - 3e^2 - 1}{2e}, \tag{46}$$

such that

$$\left(e^{A(F_n)}\right)_{jj} = \frac{(t+1)\, e^{\frac{t+1}{2}}}{2t\,(n-1)} + \frac{(t-1)\, e^{\frac{1-t}{2}}}{2t\,(n-1)} + \frac{e^2 n + n - 3e^2 - 1}{2e\,(n-1)}. \tag{47}$$

Similarly, we get

$$\left(e^{A(F_n)}\right)_{ij} = \frac{(e^t - 1)}{t} e^{\frac{1-t}{2}}. \tag{48}$$

Therefore, by substitution into $\xi_{ij}(F_n) = \left(e^{A(F_n)}\right)_{ii} + \left(e^{A(F_n)}\right)_{jj} - 2\left(e^{A(F_n)}\right)_{ij}$, we obtain the first part of the result.

For $\xi_{jj'}(F_n)$, we need expressions for the eigenvectors corresponding to the eigenvalues $\lambda_k = \pm 1$. It is easy to check that $\psi_{ki} = 0$ for $k \neq \{1, n\}$. Then, we obtain the expression for $\sum_{s=1}^{(n-1)/2} \psi_{sj}\psi_{sj'}$ where ψ_{sj} are the eigenvectors corresponding to $\lambda_s = -1$. Let $\psi_s = \left[0, \psi_{s,j_1}, -\psi_{s,j'_1}, \psi_{s,j_2}, -\psi_{s,j'_2}, \ldots, \psi_{s,j_{n-1}}, -\psi_{s,j'_{n-1}}\right]$ be one of such eigenvectors, which by normalisation provides that $2\psi^2_{s,j_1} + 2\psi^2_{s,j_2} + \ldots + 2\psi^2_{s,j_{n-1}} = 1$. Therefore, $\psi^2_{s,j_1} = 1/2 - \left(\psi^2_{s,j_2} + \ldots + \psi^2_{s,j_{n-1}}\right)$, such that we can write

$$\begin{aligned}
\sum_{s=1}^{(n-1)/2} \psi_{sj}\psi_{sj'} &= -\left(\psi^2_{s_1,j} + \psi^2_{s_2,j} + \ldots + \psi^2_{s_{(n-1)/2},j}\right) \\
&= -\left(1/2 - \left(\psi^2_{s_1,j_2} + \ldots + \psi^2_{s_1,j_{n-1}}\right) + \ldots + 1/2 - \left(\psi^2_{s_{(n-1)/2},j_2} + \ldots + \psi^2_{s_{(n-1)/2},j_{n-1}}\right)\right) \\
&= \left(\psi^2_{s_1,j_2} + \ldots + \psi^2_{s_1,j_{n-1}}\right) + \ldots + \left(\psi^2_{s_{(n-1)/2},j_2} + \ldots + \psi^2_{s_{(n-1)/2},j_{n-1}}\right) - \frac{n-1}{2}\left(\frac{1}{2}\right) \\
&= \left(\psi^2_{s_1,j_2} + \ldots + \psi^2_{s_{(n-1)/2},j_2}\right) + \ldots + \left(\psi^2_{s_1,j_{n-1}} + \ldots + \psi^2_{s_{(n-1)/2},j_{n-1}}\right) - \frac{n-1}{2}\left(\frac{1}{2}\right).
\end{aligned} \tag{49}$$

Obviously, $\sum_{s=1}^{(n-1)/2} \psi_{sj}\psi_{sj'} = -\left(\psi^2_{s_1,j} + \ldots + \psi^2_{s_{(n-1)/2},j}\right)$, such that

$$\sum_{s=1}^{(n-1)/2} \psi_{sj}\psi_{sj'} = -\left(\frac{n-1}{2} - 1\right) \sum_{s=1}^{(n-1)/2} \psi_{sj}\psi_{sj'} - \frac{n-1}{2}\left(\frac{1}{2}\right), \tag{50}$$

from which $\sum_{s=1}^{(n-1)/2} \psi_{sj}\psi_{sj'} = -\frac{1}{2}$.

Now, because $\sum_{r=1}^{(n-1)/3} \psi_{rj}\psi_{rj'} = -\psi_{1,j}\psi_{1,j'} - \psi_{n,j}\psi_{n,j'} - \sum_{s=1}^{(n-1)/2} \psi_{sj}\psi_{sj'}$, where ψ_{rj} is the eigenvector associated with $\lambda_r = 1$, we have

$$\sum_{r=1}^{(n-1)/3} \psi_{rj}\psi_{rj'} = \frac{1}{2}\left(\frac{n-3}{n-1}\right). \tag{51}$$

https://doi.org/10.1017/S0956792525000014 Published online by Cambridge University Press

Then, we can obtain

$$\left(e^{A(F_n)}\right)_{j,j'} = \frac{2e^{\frac{1+t}{2}}}{t^2-t} + \frac{2e^{\frac{1-t}{2}}}{t^2+t} + \frac{e\,(n-3)}{2\,(n-1)} - \frac{1}{2e}, \tag{52}$$

from which, by replacing in $\xi_{j,j'} = 2\left(e^{A(F_n)}\right)_{j,j} - 2\left(e^{A(F_n)}\right)_{j,j'}$ we obtain, after cancellations, that $\xi_{j,j'} = \frac{2}{e}$.

The only remaining thing to proof the result is to show that $\xi_{j,j'} < \xi_{i,j}$ for which we can easily check that

$$\xi_{i,j} - \xi_{j,j'} = \frac{n\,(t-5)+6}{2t\,(n-1)}e^{\frac{1+t}{2}} + \frac{n\,(t+5)-6}{2t\,(n-1)}e^{\frac{1-t}{2}} + \left(\frac{e\,(n-3)}{2\,(n-1)} - \frac{3}{2e}\right) > 0 \tag{53}$$

for any $n \geq 5$, which proves the result. □

The previous analytical results confirm our intuition about the identification of edges with negative curvature as arteries which communicate globally the vertices of a graph, while the edges with positive curvature are mainly those acting as capillaries connecting more local regions. For instance, while in the wheel both types of edges communicate wide regions of the graph acting as arteries and having negative curvatures, the peripheral edges in the friendship graph serve mainly as connection among the pairs of vertices forming the individual triangles and thus have positive curvature. We will return to this metaphoric interpretation later when we analyse real-world networks.

4. Total Forman–Ricci communicability curvature

Let us come back to the example of the three four cycles illustrated in Figure 2, but in this case let us consider the time at which the global consensus is reached in each of the three graphs, i.e., the time $|C_v\,(t_c) - C_v\,(t_c-1)| \leq 10^{-3}$ for all $v \in V$. We consider the initial conditions in which the concentration is allocated at every distinct vertex of the graph and then average the times at which the global steady state is reached. These times relative to the one reached for graph a) are 1.00 for a), 0.836 for b) and 1.201 for c).

We cannot focus now on the curvature of edges as we are dealing with the global steady state of the system. Let us then introduce the following.

Definition 18. *The total communicability Forman–Ricci curvature of G is defined as*

$$\mathcal{C}\,(G,\beta) := \sum_{(v,w)\in E} \mathcal{C}_{v,w}\,(G,\beta). \tag{54}$$

If we now calculate the total curvature of the edges in the three graphs under consideration, we get 0, −1.5174 and −0.1700. That is, the graph with the largest negative total curvature is the one having the fastest global diffusion. The reason is that while in b) the edge i,j has positive curvature, (j,k) and (l,i) have large negative curvatures $\mathcal{C}_{j,k}\,(b) = \mathcal{C}_{l,i}\,(b) \approx -1.611$. If we increase the weight of the edge (i,j) to three in b), then its curvature increases to 1.621, but the one of the edge (j,k) drops to −5.792, making the total curvature drops to −8.757. This is a direct consequence of the fact that the curvature is upper bounded by 2, but it can reach any negative value. Therefore, we now proceed to investigate some properties of the global Forman–Ricci communicability curvature of graphs.

We then have a corollary of Lemma 14.

Corollary 19. *Let G be a graph in which every pair of vertices is automorphically equivalent. Then,*

$$\mathcal{C}\,(G,\beta) = F\,(G), \tag{55}$$

https://doi.org/10.1017/S0956792525000014 Published online by Cambridge University Press

where $F(G) = \sum_{(v,w)\in E} F_{e=v,w}(G)$, *such that*

$$\mathcal{C}(G,\beta) = F(G) = \begin{cases} 0 & G = C_n \\ 2^{r-1} r (4-2r) & G = Q_d \\ n_1 n_2 (4 - n_1 - n_2) & G = K_{n_1,n_2} \\ n(n-1)(3-n) & G = K_n. \end{cases} \tag{56}$$

Let us now consider the path graph with n vertices P_n. Let $\beta = 1$ and let us designate $\mathcal{C}(G, \beta = 1) = \mathcal{C}(G)$. In this case, we have that $\xi_{i,i+1}(P_n)$ for $i \leq n/2$ (n even) or $i \leq (n+1)/2$ (n odd) [20] is given by

$$\xi_{i,i+1}(P_n) = 2I_0(2) - 2I_1(2) - I_{2i}(2) - I_{2(i+1)}(2) + 2I_{2i+1}(2). \tag{57}$$

Then, if we label the vertices from one end of the path from 1 to n, we can obtain the curvatures of each edge analytically. For instance,

$$\mathcal{C}_{1,2}(P_n) = 2 - \sqrt{\frac{2I_0(2) - 2I_1(2) - I_2(2) - I_4(2) + 2I_3(2)}{2I_0(2) - 2I_1(2) - I_4(2) - I_6(2) + 2I_5(2)}} \approx 1.1108. \tag{58}$$

Similarly, we have

$$\mathcal{C}_{2,3}(P_n) \approx -0.1131, \tag{59}$$

$$\mathcal{C}_{3,4}(P_n) \approx -0.0112, \tag{60}$$

$$\mathcal{C}_{4,5}(P_n) \approx -4.3573 \cdot 10^{-4}, \tag{61}$$

$$\mathcal{C}_{5,6}(P_n) \approx -7.7712 \cdot 10^{-6}, \tag{62}$$

$$\mathcal{C}_{6,7}(P_n) \approx -8.9148 \cdot 10^{-8}, \tag{63}$$

and so forth.

It can be seen that

$$\lim_{i\to\infty} \xi_{i,i+1}(P_n) = 2I_0(2) - 2I_1(2), \tag{64}$$

and

$$\lim_{i\to\infty} \mathcal{C}_{i,i+1}(P_n) = 2 - \lim_{i\to\infty} \left(\sqrt{\frac{\xi_{i,i+1}(P_n)}{\xi_{i,i-1}(P_n)}} + \sqrt{\frac{\xi_{i,i+1}(P_n)}{\xi_{i+1,i+2}(P_n)}} \right) = 0, \tag{65}$$

which is obviously reached when $n \to \infty$. Indeed, it can be easily checked that for $i \geq 7$:

$$\left(\sqrt{\frac{\xi_{i,i+1}(P_n)}{\xi_{i,i-1}(P_n)}} + \sqrt{\frac{\xi_{i,i+1}(P_n)}{\xi_{i+1,i+2}(P_n)}} \right) < 10^{-9}. \tag{66}$$

Therefore, we can obtain an approximation for $\mathcal{C}(P_n)$ by considering only the contributions from $1 \leq i \leq 6$. That is, for any P_n with $n \geq 12$ we have (see Table 3)

$$\mathcal{C}(P_n) = 2 \sum_{i=1}^{k \ll n/2} \mathcal{C}_{i,i+1}(P_n) \approx 1.97213365 \ldots. \tag{67}$$

https://doi.org/10.1017/S0956792525000014 Published online by Cambridge University Press

Table 3. *Values of the Forman–Ricci communicability curvature for path graphs with n vertices as computed by using Matlab*

n	$\mathcal{C}(P_n)$
2	2.0000
3	2.0000
4	1.9777
5	1.9726
6	1.9722
7	1.972134412331060
8	1.972133670041003
9	1.972133652650161
10	1.972133652345863
20	1.972133652341688
50	1.972133652341688

For $n < 12$, we are adding less negative terms from $\mathcal{C}_{1,2}(P_n)$ in the formula for $\mathcal{C}(P_n)$, such that we can conclude that $\mathcal{C}(P_n) > 0$ for any $n \geq 2$.

To investigate the importance of the characterisation of global curvature in graphs, we consider again the toy models introduced in the previous section where we have studied the communicability curvatures of edges in wheel W_n and friendship F_n graphs on n vertices. Let us then consider here the mean edge curvature in these graphs, which can be written as

$$\bar{\mathcal{C}}(W_n) = \frac{1-n}{2} - \sqrt{\frac{\xi_{i,j}(W_n)}{\xi_{j,j'}(W_n)}} - \sqrt{\frac{\xi_{j,j'}(W_n)}{\xi_{i,j}(W_n)}}, \tag{68}$$

and

$$\bar{\mathcal{C}}(F_n) = \frac{2}{3}\left(2-n - \sqrt{\frac{\xi_{i,j}(F_n)}{\xi_{j,j'}(F_n)}} - \sqrt{\frac{\xi_{j,j'}(F_n)}{\xi_{i,j}(F_n)}}\right). \tag{69}$$

Then, let $a := \sqrt{\frac{\xi_{i,j}(W_n)}{\xi_{j,j'}(W_n)}} + \sqrt{\frac{\xi_{j,j'}(W_n)}{\xi_{i,j}(W_n)}}$ and $b := \sqrt{\frac{\xi_{i,j}(F_n)}{\xi_{j,j'}(F_n)}} + \sqrt{\frac{\xi_{j,j'}(F_n)}{\xi_{i,j}(F_n)}}$, so that we can write

$$\bar{\mathcal{C}}(W_n) - \bar{\mathcal{C}}(F_n) = \frac{n-5}{6} + \frac{2b-3a}{3}, \tag{70}$$

which can be either negative or positive depending on how large a and b are for the different sizes of these graphs. It can be seen that $\xi_{ij}(W_n)$ and $\xi_{ij}(F_n)$ grow with n while $\xi_{jj'}(W_n)$ and $\xi_{jj'}(F_n)$ remain constant. Therefore, the curvatures of the j, j' edges remain constant for very large n

$$\lim_{n\to\infty} \sqrt{\frac{\xi_{jj'}(W_n)}{\xi_{ij}(W_n)}} = 0, \tag{71}$$

and

$$\lim_{n\to\infty} \sqrt{\frac{\xi_{jj'}(F_n)}{\xi_{ij}(F_n)}} = 0. \tag{72}$$

Both distances, $\xi_{i,j}(W_n)$ and $\xi_{i,j}(F_n)$ grow with n. It is expected that $\xi_{i,j}(W_n) < \xi_{i,j}(F_n)$ for very small graphs because the surrounding periphery (edges (j, j')) facilitates the communication around the graph, without increasing too much the mean shortest path distance of the graph. For instance, every pair of

https://doi.org/10.1017/S0956792525000014 Published online by Cambridge University Press

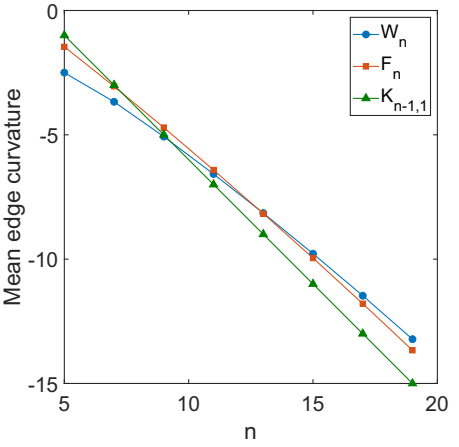

Figure 4. *Scatterplot of the mean communicability curvature of wheel W_n, friendship F_n and star $K_{n-1,1}$ graphs with different number of vertices n. The lines are drawn to guide the eye. All the calculations were performed by using $\beta = 1$.*

vertices in W_5 can be communicated by peripheric edges in no more than two steps, and in W_3 by no more than 3. However, this advantage disappears when the size of the graphs increase because in these cases, going around the graph by peripheric edges can be a handicap to communicate pairs of vertices. Consequently, it is expected that when n grows $\xi_{i,j}(W_n) > \xi_{i,j}(F_n)$, and there should be a crossing in the curves indicating the changes of $\bar{C}(W_n)$ and $\bar{C}(F_n)$ vs. n. The same reasoning can be applied to the star graphs $K_{n-1,1}$, in which there are no peripheric edges at all. Then, it is expected that the star graph become the one with the edges with the most negative curvature as n grows. This is exactly what is observed when we plot the average edge curvatures for the three types of graphs in Figure 4, where it can be seen that a wheel graph has, as average, the most negative edge curvature for small sizes but less negative ones for larger size relative to the friendship graphs of the same sizes. For large n, the star graphs have the most negative average curvature of all the three graphs. This results indicates that only relative short peripheric paths can be considered as 'bypasses' that really make the average curvature of a graph more negative. Such bypasses have been investigated previously as facilitators of the navigability of a network [26].

5. Applications

When a new concept, like the communicability curvature of edges, is introduced in network theory, it is important to provide some insights about the kind of information that it provides and some indications about the areas in which it can be used. In a conceptual work as the current one, it is impossible to make an exhaustive exploration of these two important tasks, which are left for further works in specific application areas. Therefore, the main goal of this section is to provide such insights about the structural meaning of the communicability curvature of edges and what kind of information it can provide to researchers in complex network theory. For that purpose, we select here three examples to illustrate some potential areas in which the Forman–Ricci communicability curvature can be applied to the study of real-world networks. The first of these networks is that representing the US airport transportation network as in 1997 [5]. This network consists of 332 airports in continental US, Alaska and overseas territories. The network contains 2126 undirected edges representing the existence of flight connections between the corresponding pair of airports. The second network represents a version of the neuronal network of the worm *C. elegans*, which is formed by 277 vertices representing the neurons in this organism

https://doi.org/10.1017/S0956792525000014 Published online by Cambridge University Press

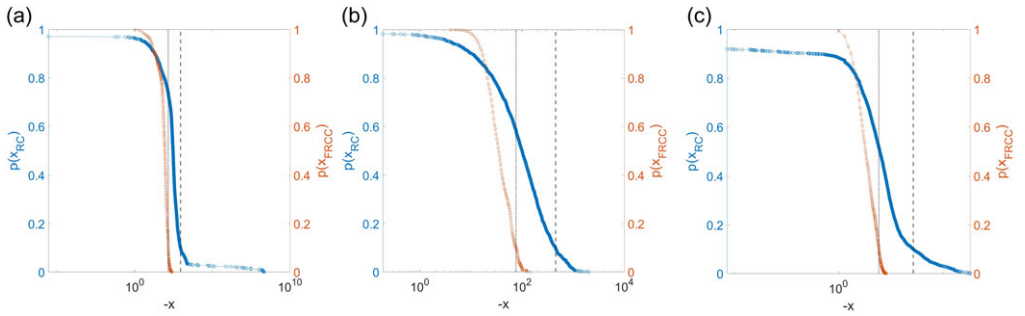

Figure 5. *Cumulative probability distributions (CDF) of the curvatures (RC as red squares and FRCC as blue circles) for the three real-world networks studied here: a) USA airport transport network, b) neuronal network of C. elegans, c) collaboration network in computational geometry. In the plots, we represent only the negative curvatures which are given as $-x$, the right scale is for FRCC and the left is for RC. The vertical bars represent the curvatures marking the top 10% of the most negative ones (those to the right of the respective lines).*

and 1918 edges which represent the existence of synaptic connection (chemical or electrical) between the corresponding pair of neurons [14]. The original dataset consisting of the electron micrograph reconstruction of the worm nervous system consisted of 302 neurons [59]. However, we use here the version published in 2004 [14] due to the following reasons. As remarked recently by Skuherski et al. [54], the original 302 neurons atlas can lead to unlabelled and even mislabelled neurons due to the density of neurons in various ganglia and ambiguities in atlas matching that are present as a result. The 2004 atlas, used here, is the one commonly used in papers that make use of *C. elegans* neuron positions, which is also the case of the current work. Although the original network is directed, we consider here its undirected version. Finally, we consider a collaboration network in the area of computational geometry. The version of the network studied here is taken from [5] and it is based on the file geombib.bib that contains Computational Geometry Database, version February 2002, where the vertices represent authors in the area of computational geometry and two vertices are connected if the corresponding authors have published a paper together according to the BibTeX bibliography obtained from the Computational Geometry Database geombib, version February 2002. The dataset was cleaned by Pajek project [5] such that different versions of the same name are merged together under one single name. The clean network contains 7343 vertices and 11,898 edges. Here, we consider the giant connected component of this network, which consists of 3621 authors and 9461 coauthorship relations.

In this section, all calculations are performed by considering the use of $\beta = 1$. We start by calculating the Forman–Ricci communicability curvature (FRCC) as well as the unweighted Forman–Ricci curvature (RC) for every edge in the three networks. In Figure 5, we plot the distributions of both curvatures for the three networks under study. The most important feature of these distributions is the fact that FRCC covers an extremely wider range of values than RC. For instance, in the airport network, FRCC have values in the range between -10^8 and 2 (mean $-1.94 \cdot 10^6$), while RC ranges between -253 and -1 (mean -3.26). In the neuronal network, FRCC ranges between -10^3 and 2 (mean -178.37), while RC has values between -81 and 3 (mean -2.03). Finally, the network of collaboration in computational geometry shows values of FRCC between -10^6 and 2 (mean $-1.94 \cdot 10^4$), while RC goes between -196 and 1 (mean -0.0474). Hereafter, we will consider the most negative values of the curvatures as a way to analyse which kind of information is contained in such extreme tails of the distributions.

Notice that because we are considering the curvatures as a kind of edge centrality, we are then mainly interested in the most central edges only, which here means those with the most negative curvatures. Therefore, we selected the edges in the top 10% of the most negative curvatures for each of the two measures. Then, for each of the three examples, we constructed the networks formed by all the vertices and the edges selected in this top 10% of most negative curvatures. That is, we are interested in

https://doi.org/10.1017/S0956792525000014 Published online by Cambridge University Press

Table 4. *Comparison between the number of connected components (NCC) and the size (number of vertices) in the largest connected component (SLCC) formed by the edges with the top 10% of highest Forman–Ricci communicability curvature (FRCC) and of the Ricci curvature (RC) for the three real-world networks studied in this work*

	FRCC				RC				Real		
Network	NCC	SLCC	$\bar{k}$	k_{max}	NCC	SLCC	$\bar{k}$	k_{max}	n	$\bar{k}$	k_{max}
US airports	158	155	2.49	58	226	107	4.19	106	332	12.81	139
Neurons	147	131	2.93	44	177	101	3.82	76	277	13.84	76
Collaboration	2878	162	3.38	22	3265	357	5.34	102	3621	5.22	102

investigating the global connectivity of the subgraph which contains the edges in the top 10% of curvatures. In particular, we investigate the number of connected components (NCCs) and the size of the largest connected component (SLCC) in these subgraphs. The results are given in Table 4, where we also give the mean degree ($\bar{k}$) and maximum degree (k_{max}) of the vertices in the largest connected component (LCC). For the three networks, the subgraph formed by the edges in top 10% of FRCC are more connected than those in the corresponding subgraph obtained for RC. For instance, in the airport network of USA, the top 10% of FRCC edges form 156 components, while those in the top 10% RC are distributed in 226 components. In the case of the neuronal network, the top 10% of RC edges are distributed in 30 components more than those based on FRCC. Finally, in the collaboration network, there are 387 more components in the RC subgraph than in the FRCC one. The SLCC in the airport and neuronal networks are bigger for the FRCC than for RC, which in the collaboration network this is significantly bigger for RC than for FRCC. In the three cases, the average degree and the maximum degree of the vertices in the LCC are smaller for FRCC than for RC. It is important to remark that the LCC formed by RC resembles more the subgraph formed by the most connected vertices in the graph than the one formed by FRCC. This can be seen in the fact that the LCC formed by the edges in the top 10% by RC have very similar maximum degree than those in the real graph (see Table 4), which coincide in the cases of neurons and collaboration networks.

In closing, the top 10% of edges in the FRCC form a significant different subgraph than the one formed by those in the RC ranking. In general, edges in the top ranking by FRCC form a more connected subgraph expressed by a smaller number of connected components. Also, the LCCs formed by the top 10% edges ranked by the two curvatures are significantly different, with those formed by RC resembling more a 'rich club' containing the pairs of vertices with the largest degree in the respective graphs.

An important consequence of the differences remarked before between the top edges in the FRCC and RC rankings is related to the robustness of these networks to the failure of these edges. For instance, if we remove the edges in these top 10% of FRCC and RC rankings, we obtain in general very different networks. For instance, let us remove these edges in the top 10% of RC in the network of the US airports. The remaining network is still a connected graph, i.e., it has only one connected component formed by the 332 vertices of the original network. On the contrary, if we remove the same number of edges, but now those in the top 10% of FRCC ranking, the network is chopped into 23 connected components, the largest one containing 282 vertices. The difference between removing the top 10% of edges by their FRCC and RC rankings in the neuronal network is not significant. While the removal by RC does not increases the NCC, the one by FRCC splits the network into two connected components, but the largest one contains 99.3% of the vertices of the network. This is possibly due to the fact that this network is relatively highly dense in comparison with the other two. In the case of the collaboration network, the removal by RC splits the network into 101 CC, the largest of which retains 96.8% of the vertices in the original graph. However, the removal of the same number of edges based on FRCC splits the network into 170 CC, which represents 40% of increment relative to RC. Also importantly, the damage made by the removal based on FRCC to the LCC is more significant than the one made by RC because the

https://doi.org/10.1017/S0956792525000014 Published online by Cambridge University Press

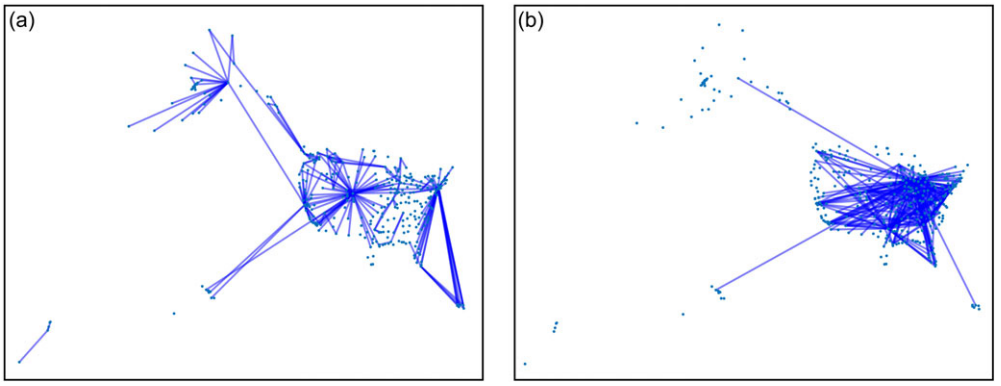

Figure 6. *Illustration of the edges with the most negative FRCC (a) and RC (b) in the network of airline connections among the US airports.*

first retains only 86% of the vertices of the original graph, which is 10% less than that left by the RC removal. All in all, it seems that edges with large negative FRCC represent more important connections than those based on RC for the robustness of the networks relative to edges failures. Although more systematic studies are needed for a large pool of networks, it seems that 'protecting' edges with large FRCC is a good strategy to protect the failures of networks to edge removals.

We now study in more detail the characteristics of those edges in the top rankings by FRCC and RC in the three networks studied here.

5.1 Airport network of USA

The plots in Figure 6 illustrate the airport connections in the top 10% most negative curvatures according to FRCC (a) and RC (b). There is an obvious difference between the two subgraphs containing those edges in the top 10% by FRCC and RC. The LCC formed by the edges in the top 10% of RC is strongly dominated by the major hub(s) of the airport network. For instance, 47% of all the edges in the LCC of this graph are formed by connections involving Chicago O'Hare International airport. Some of these connections are with other of the major hubs like Dallas/Fort Worth Intl., The William B Hartsfield Atlanta, Pittsburgh Intll., Lambert-St Louis Intl., Charlotte/Douglas Intl. and Stapleton Intl. But this is not only the case, as the connections between Chicago's airport and some others poorly connected ones like Lehigh Valley Intll., Eagle County Regional, Columbia Metropolitan and others also appear among the top RC edges. This is due to the fact that RC between two vertices i and j is $4 - k_i - k_j$, such that if at least one of the vertices is of large degree, the curvature will be highly negative.

In contrast, the top FRCC edges are not dominated by any of the airports in the top six of connectivity, but by the Stapleton International airport which is the seventh according to its number of connections in this version of the USA airport network. The Stapleton International airport appears in the LCC of the FRCC ranking together with 35 edges incident to it. Then, it is followed by Anchorage International and Newark International, both with 14, and then, we find the airports of Missoula International and Billing Logan International, both with 9 connections in the top of most negative curvatures. As we have seen before these airports generate a more connected network than the one formed by the top RC edges, indicating that they may play a fundamental role in the large scale connectivity of this network.

A close inspection of the edges having the most negative FRCC reveals that in general they are formed by an important hub of the air transportation network of USA and a local/regional airport. For instance, some of the most negative edges appears between Stapleton Intl., which is a hub and the airports of Walker Field, Santa Barbara Muni, Long Beach /Daugherty Field/, Springfield Regional, Gunnison County, Aspen-Pitkin Co/Sardy Field and Fresno Air Terminal. Similarly, highly negative

https://doi.org/10.1017/S0956792525000014 Published online by Cambridge University Press

edges are formed between Newark Intl. and the airports of Rafael Hernandez, Mercedita, Alexander Hamilton, Daytona Beach Intl, Melbourne Intll, Cyril E King, Columbia Metropolitan, as well as between Anchorage and Dillingham, King Salmon, Port Heiden, Sand Point, Unalaska and Adak Naf. Let us remind here that the curvature of the edge (i,j) is obtained by subtracting from 2, the sum of the ratios $\tilde{\xi}_{ij}/\tilde{\xi}_{ir} + \tilde{\xi}_{ij}/\tilde{\xi}_{jk}$, where $\tilde{\xi}_{ij} = \sqrt{\xi_{ij}}$, r is a vertex adjacent to i and k is a vertex adjacent to j. Let us consider, for instance, the edge Walker Field to Stapleton Intl. The airport of Walker Field is the third largest one in Colorado, while Stapleton Intl. in Denver is the largest one. Between April 2022 and March 2023, the Walker Field moved about 230,000 passenger, from which 100,000 were moved to Stapleton. The main difference is that Stapleton is one of the major hubs of the US airport transportation system, which is also directly connected to other major hubs, like Chicago O'Hare, Dallas Forth Worth, La Guardia, San Francisco Intl., JFK, La Guardia, etc. Let us consider that $i =$ Stapleton Intl, $j =$ Walker Field and $r =$ Newark Intl., which is one of the hubs connected to Stapleton. We can see that $\tilde{\xi}_{ij}/\tilde{\xi}_{ir} = 1837.9$, which already makes $\mathcal{C}_{ij} \leq -1835.9$, which is a very negative curvature for this edge. Obviously, if we consider now the triple $i =$ Newark Intl, $j =$ Rafael Hernandez, which is the second largest airport in Puerto Rico, and $r =$ Stapleton, a hub connected to Newark, we obtain $\tilde{\xi}_{ij}/\tilde{\xi}_{ir} = 1758.0$, which give a highly negative curvature for the edge Newark-Rafael Hernandez, i.e., $\mathcal{C}_{ij} \leq -1756$. The explanation of the large negative curvature of edges involving the airport of Anchorage is relatively different. It comes from the fact that $\tilde{\xi}_{ij}$, where $i =$ Anchorage, $j =$ local airport 1, is significantly bigger than $\tilde{\xi}_{jk}$ where $k =$ local airport 2. For instance, if $i =$ Anchorage, $j =$ Dillingham and $k =$ King Salmon, then $\tilde{\xi}_{ij}/\tilde{\xi}_{jk} \approx 2.91 \cdot 10^7$, which makes the curvature of the edge Anchorage Dillingham an extremely negative one. The reason for this effects is that Alaska works as a more isolated 'ecosystem' than the one formed by continental airports. Then, many local airports have a direct connection with Anchorage, but they also share some connections among them. Then, what happens is that Anchorage acts like the major hub to which some local small 'hubs' connect other airports, such as the case of the airport of Dillingham, which is connected to the one of King Salmon. All in all, the negative edges in the airport transportation system of USA are the arteries of the system formed by connections between local airports and some hubs which allow the global connection of these local/regional airports with other major hubs of the network. No surprise then that their removal makes a bigger damage to the network structure than removing the edges in the top 10% of most negative RC as we have seen before.

Let us now turn our attention towards those edges which have positive curvature in the US airport network. There are 57 edges with $\mathcal{C}_{ij} > 0.2$, from which 52 correspond to interregional connections. That is, more than 91% of the edges with positive curvature involve pairs of regional airports, either in the same or in different regions of the USA, similar to what capillaries do inside the same organ in the body. For instance, the edge corresponding to airports Williamson County Regional and Cape Girardeau Regional has curvature of approximately 2, which is the maximum that an edge can have. They connect the regions of Southern Illinois and that of in Scott County, in Missouri. However, the edge connecting Port Heiden and Sand Point, which has curvature also of approximately 2, connects two regions in Alaska. Therefore, the edges with positive curvature clearly points to to connections between pairs of local/regional airports among them. The exceptions to this rule are the pairs: Palm Spring-Tucson Intl., Newark-Stapleton, Portland Intll.-San Jose Intll., JFK-McCarran Intl. and San Francisco Intl.-Miami Intll. These five pairs of airports mainly correspond to major or mid-size hubs of the network. Their main characteristic is that they form pairs of relatively similar airports in terms of their connectivity as well as in their capacity for moving passengers. For instance, Palm Spring has degree equal to 13, very similar to Tucson which has degree equal to 14. Newark and Stapleton have degrees of 67 and 85, respectively, and they moved in 1997 (the year of the version of this network) 30 and 34 millions of passengers, respectively. JFK and McCarran Intl. have degrees equal to 46 and 49, respectively, and move 45–62 millions and 48–57 millions of passengers, respectively. San Francisco Intl. and Miami Intl. have degrees of 68 and 47, respectively, and move about 41 and 33 millions of passengers in 2000. In closing, the positive curvature of edges in the US airport network indicate those pairs of airports with very similar connectivity and passenger capacities, which are typical of regional–regional pairs as well as of some mid-size and major hubs in the network.

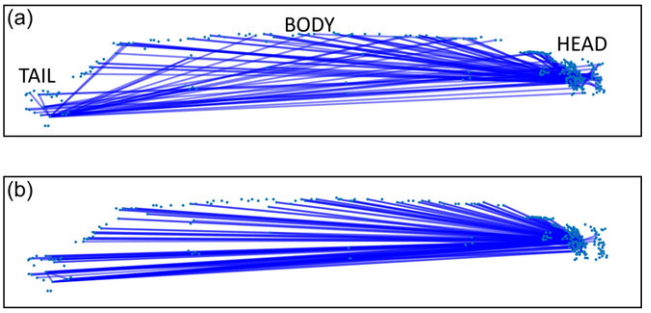

Figure 7. *Illustration of the edges with the most negative FRCC (a) and RC (b) in the network of synaptic connections among neurons in the worm C. elegans.*

5.2 Neuronal network of C. elegans

In Figure 7, we illustrate the neuronal connections in the top 10% most negative curvatures according to FRCC (a) and RC (b). While for FRCC, there are 1885 edges with negative curvature, with average of -181.50, and 33 edges with positive curvature, averaging 0.814, for RC all the edges have negative curvature, which averages -40.62. As in the previous example here again, the edges with the most negative RC are formed by pairs of vertices of the largest degree. For instance, more than 76% of these edges are formed by interconnections of the neurons AVAL (76 connections) and AVAR (72 connections) with neurons of large degree like AVBR, AVEL, PVCR, AVBL, PCVL, AVER, AVDR, AVBR, etc. AVA neurons are command interneurons, which are located at the lateral ganglia of head (L for left and R for right location). Notice that the edge with the most negative RC is the one connecting these two neurons: AVAL-AVAR. Many of the neurons with the largest negative RC which have connections with AVA ones are also located at the lateral ganglia of the head (AVBR, AVEL, AVBL, AVER, AVDR, AVBR), but there are also others located in the tail, like PVCR and PVCL. 98% of the edges in the top 10% of most negative ones according to RC involve a neuron located in the head of the worm. In Figure 8(a), we can observe that there are neither connections involving two neurons located at the body nor two neurons both located in the tail, and that only 2.1% of connections involve body–tail regions.

There is a significant difference in these percentages for most negative edges according to the FRCC. As can be seen in Figure 8(b), there is significant percentage of negative edges which involve pairs of neurons both located at the body or at the tail of the worm. More important are the differences provided by the edges with negative and positive curvature. It is known that the nerve ring in the head of *C. elegans* groups the majority of the neurons and synapses of the worm. Therefore, it is not surprising that most of the edges with high negative curvature (49%) as well as of those with positive one (57.6%) are wiring neurons located in the head of *C. elegans*. However, as can be seen in Figure 8, almost 27% of the connections with very negative curvature occurs between neurons located in the head with others in the mid body of the worm. This percentage grows up to 37.6% if we consider together neurons with locations of types h–b and h–t. It is also significant that the b–t connections represent 7.4% of the total number of edges at the top ranking of negative curvature. Contrastingly, one-third of the edges with positive curvature connect neurons located in the mid body of the worm, i.e., b–b connections, with only one edge connecting head to body and another connecting head to tail and no edge connecting body and tail.

5.3 Collaboration network in computational geometry

We now focus on the collaboration network in computational geometry. In this case, the percentages of negative edges according to both curvatures are similar: 94.4% for RC and 92% for FRCC. The non-negative RC edges are formed by 442 edges with zero RC and 103 edges with RC equal to one. We now

https://doi.org/10.1017/S0956792525000014 Published online by Cambridge University Press

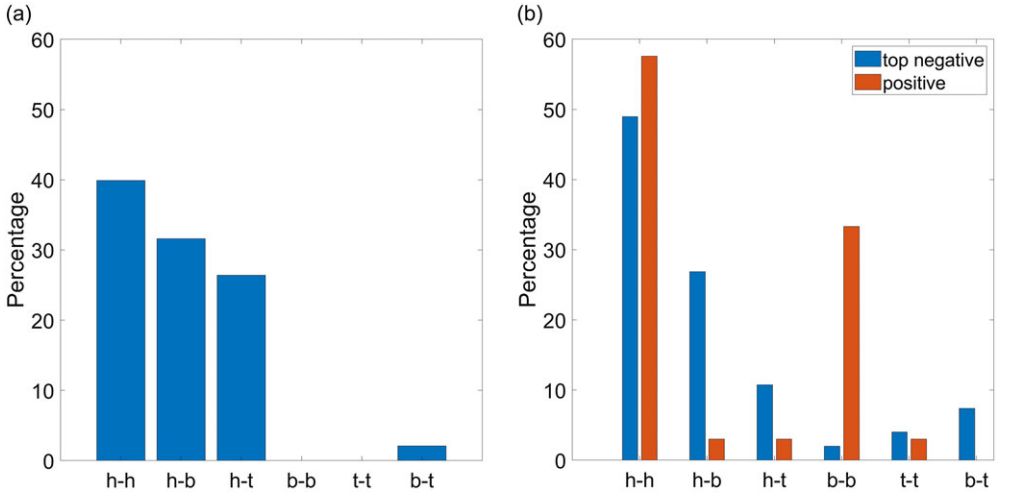

Figure 8. *Percentage of edges with communicability curvature among the most negative (blue) and positive ones (red) that connect pairs of neurons both in the head (h–h), head–body (h–b), head–tail (h–t), two in the body (b–b), the two in the tail (t–t) and body–tail (b–t) using RC (a) and FRCC (b). The network does not have positive edges according to RC.*

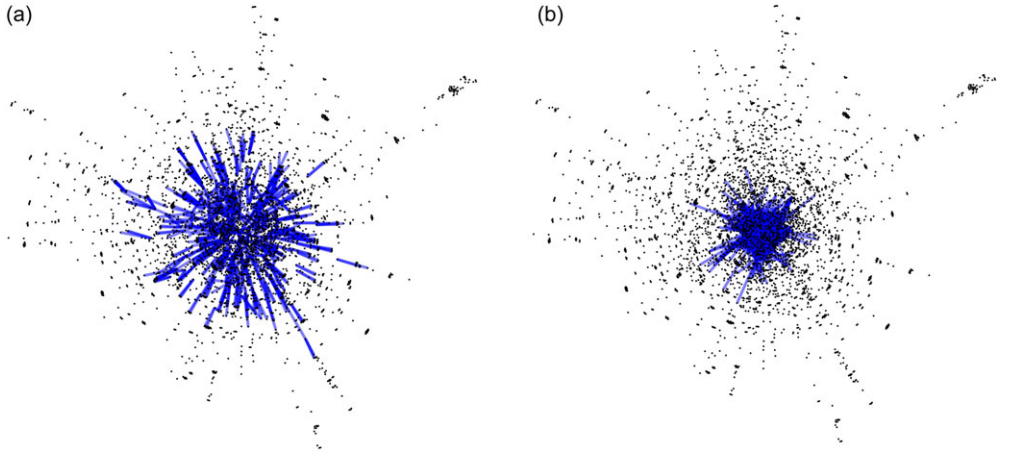

Figure 9. *Illustration of the edges with the most negative RC (a) and FRCC (b) of the collaboration network in computational geometry.*

compare the collaborations existing in the top 10% of edges ranked by their RC and FRCC (see Figure 9). We have seen before that in this network, the LCC formed by the most negative edges according to RC is bigger than that formed by FRCC (see Table 4). As can be seen in Figure 9, the most negative edges according to RC form a significantly more compact core than the ones according to FRCC. For instance, the edges in the top 10% of FRCC are grouped into 169 cliques of sizes between 5 and 11. There are two cliques of size 11, which are formed by some of the most connected authors in this network (degree is given in parenthesis): Agarwal (98), O'Rourke (85), Tamasia (79), Dobkin (73), Goodrich (70), Suri (63), Sack (61), Whitesides (59), Preparate (53), Vitter (53) and Chen (41). Among the 18 cliques with 8 authors, we find Guibas (102), Agarwal (98), Snoeyink (91), Edelsbrunner (90), Overmars (98), Yap (76), Dobkin (73) and Eppstein (61). The LCC of this network resembles a core-satellite graph [25], in which some authors coparticipate in several cliques of smaller size.

https://doi.org/10.1017/S0956792525000014 Published online by Cambridge University Press

In contrast, the top 10% of edges ranked by FRCC does not form any clique of length three or higher. These edges do not include, in general, connections between the major hubs of the network as in the case of RC. Instead, it includes in the very top ranking the connections of some of the major hubs and a few of their collaborators, who also collaborate among them. For instance, Guibas (102) has collaborated with Harer, Grimm, Zorin, Weeks, Johnson, Sedwick and Hicks, who also have collaborated among them forming a clique. Then, the connections between Guibas and each of these authors are among the top most negative edges by FRCC. The same happens for these collaborators, all of which have degree 21, with other main authors like Agarwal (98), Edelsbrunner (90), Yap (76) and Dobkin (73). The positive edges are then, in general, those connecting some of these coauthors. It should be remarked that the collaborator–collaborator edges not always have positive RCC, but in many occasions they also display negative FRCC with relatively small magnitude. In this scenario, the main hubs and their collaborators form the arteries of the system while the collaborator–collaborator edges form the capillaries.

At the end of this section of applications, we would like to remark that the communicability curvature is not trivially related to the unweighted Forman–Ricci curvature which only contains local information about a given edge. In fact, for the three real-world networks analysed, both measures are very poorly correlated to each other, i.e., the Pearson correlation coefficients between them are 0.013 (USA airports), 0.497 (*C. elegans* neurons), and 0.193 (collaboration network).

6. Conclusions

The Forman–Ricci communicability curvature displays several important characteristics to be used for the analysis of graphs and networks. First, it is a local invariant which contains information about the global influence of the network on a particular edge. Therefore, it is not trivially related to the unweighted Forman–Ricci curvature which only contains local information about a given edge. In fact, for the three real-world networks analysed both measures are very poorly correlated to each other. Second, it is directly related to diffusive dynamical models on graphs, which allows to investigate structure–function relations in networks. Last, but not least, it is directly related to the spectrum of the adjacency matrix via the communicability distance function, which allow many further explorations connecting geometric parameters with algebraic graph theory.

As we have seen from the analysis of the real-world examples considered here, the communicability curvature based on Forman–Ricci discrete curvature accounts for significant differences in the functional role of edges in networks. While edges with very large negative curvature allow the communication between important hubs with ‘peripheral‘ vertices, the edges with positive curvature represent a vasculatory framework of connections between these second class of vertices (and sometimes between hubs) in the network.

Two main handicaps of the Forman–Ricci communicability curvature are the following. While this curvature can take any negative value for an edge, it is upper bounded by a positive curvature of 2. This makes that the values of the edge curvature are extremely asymmetric favouring the dominance of negative ones. This is inherent to the definition of the Forman–Ricci curvature. Thus, we suggest to explore other definitions, like the one given in refs. [15, 16] using the communicability distance instead of the resistance one. The second problem is the extension of the Forman–Ricci communicability curvature to directed graphs. Although the original definition allows such extension, the communicability distance is, like any distance, a symmetric function. Therefore, other approaches based more on the communicability ‘flow‘ instead of the distance should be explored here.

Acknowledgements. The author was motivated by this topic during his visit to Max Planck Institute for Mathematics in the Sciences, Leipzig, where the discussions with Prof Jost and Dr Restrepo were very illuminating. Special thanks are given to Dr A. A García-Chung for helpful comments and discussions on the specific content of this work. The conscious and constructive revision of this work by two anonymous referees is also sincerely thanked.

Competing interests. The author declares that he has no competing interests.

References

[1] Asllani, M., Da Cunha, B. R., Estrada, E. & Gleeson, J. P. (2020) Dynamics impose limits to detectability of network structure. *New J. Phys.* **22**(6), 063037.
[2] Avena-Koenigsberger, A., Misic, B. & Sporns, O. (2018) Communication dynamics in complex brain networks. *Nat. Rev. Neurosci.* **19**(1), 17–33.
[3] Bakry, D. & Émery, M. (2006) Diffusions hypercontractives. In *Séminaire de Probabilités XIX 1983/84: Proceedings*. Springer, pp. 177–206.
[4] Balaji, R. & Bapat, R. B. (2007) On Euclidean distance matrices. *Linear Algebra Appl.* **424**(1), 108–117.
[5] Batagelj, V. & Mrvar, A. (2006) Pajek datasets. http://vlado.fmf.uni-lj.si/pub/networks/data/mix.USAir97.net.
[6] Bauer, F., Jost, J. & Liu, Sh (2012) Ollivier-Ricci curvature and the spectrum of the normalized graph laplace operator. *Math. Res. Lett.* **19**(6), 1185–1205.
[7] Benzi, M. & Boito, P. (2020) Matrix functions in network analysis. *GAMM-Mitteilungen* **43**(3), e202000012.
[8] Bochner, S. (1948) Curvature and betti numbers. *Ann. Math.* **49**(2), 379–390.
[9] Boguñá, M., Bonamassa, I., De Domenico, M., Havlin, S., Krioukov, D., Serrano, M.Á. (2021) Network geometry. *Nat. Rev. Phys.* **3**(2), 114–135.
[10] Burago, D., Burago, Y., Ivanov, S., et al. (2001) *A Course in Metric Geometry*, Vol. **33**. Providence, RI, American Mathematical Society.
[11] Chatterjee, T., Albert, R., Thapliyal, S., Azarhooshang, N. & DasGupta, B. (2021) Detecting network anomalies using forman–ricci curvature and a case study for human brain networks. *Sci. Rep. UK* **11**(1), 8121.
[12] Chatterjee, T., DasGupta, B. & Albert, R. (2021) A review of two network curvature measures. *Nonlinear Anal. Global Optimiz.* **167**, 51–69.
[13] Chen, I., Benzi, M., Chang, H. H. & Hertzberg, V. S. (2016) Dynamic communicability and epidemic spread: A case study on an empirical dynamic contact network. *J. Complex Netw.* **5**(2), 274–302.
[14] Choe, Y., McCormick, B. H. & Koh, W. (2004) Network connectivity analysis on the temporally augmented C. elegans web: A pilot study. In *Society for Neuroscience*, Vol. **30**
[15] Devriendt, K. & Lambiotte, R. (2022) Discrete curvature on graphs from the effective resistance. *J. Phys. Compl.* **3**(2), 025008.
[16] Devriendt, K., Ottolini, A. & Steinerberger, S. (2024) Graph curvature via resistance distance. *Discrete Appl. Math.* **348**, 68–78.
[17] Dokmanic, I., Parhizkar, R., Ranieri, J. & Vetterli, M. (2015) Euclidean distance matrices: Essential theory, algorithms, and applications. *IEEE Signal Process. Mag.* **32**(6), 12–30.
[18] Eckmann, J.-P. & Moses, E. (2002) Curvature of co-links uncovers hidden thematic layers in the world wide web. *Proc. Natl. Acad. Sci.* **99**(9), 5825–5829.
[19] Elkin, R., Oh, J. H., Dela Cruz, F., Norton, L., Deasy, J. O., Kung, A. L., Tannenbaum, A. R. (2024) Dynamic network curvature analysis of gene expression reveals novel potential therapeutic targets in sarcoma. *Sci. Rep. UK* **14**(1), 488.
[20] Estrada, E. (2012) The communicability distance in graphs. *Linear Algebra Appl.* **436**(11), 4317–4328.
[21] Estrada, E. (2012) *The Structure of Complex Networks: Theory and Applications*, Oxford, Oxford University Press.
[22] Estrada, E. (2024) What is a complex system, after all? *Found. Sci.* **29**(4), 1143–1170.
[23] Estrada, E. (2024) Communicability cosine distance: Similarity and symmetry in graphs/networks. *Comput. Appl. Math.* **43**(1), 49.
[24] Estrada, E. (2024) Conservative vs. non-conservative diusion towards a target in a networked environment. In *The Target Problem*. Springer, Berlin.
[25] Estrada, E. & Benzi, M. (2017) Core–satellite graphs: Clustering, assortativity and spectral properties. *Linear Algebra Appl.* **517**, 30–52.
[26] Estrada, E., Gómez-Gardeñes, J. & Lacasa, L. (2023) Network bypasses sustain complexity. *Proc. Natl. Acad. Sci.* **120**(31), e2305001120.
[27] Estrada, E. & Hatano, N. (2007) Statistical-mechanical approach to subgraph centrality in complex networks. *Chem. Phys. Lett.* **439**(1-3), 247–251.
[28] Estrada, E. & Hatano, N. (2008) Communicability in complex networks. *Phys. Rev. E* **77**(3), 036111.
[29] Estrada, E. & Hatano, N. (2016) Communicability angle and the spatial efficiency of networks. *SIAM Rev.* **58**(4), 692–715.
[30] Estrada, E., Hatano, N. & Benzi, M. (2012) The physics of communicability in complex networks. *Phys. Rep.* **514**(3), 89–119.
[31] Estrada, E. & Rodriguez-Velazquez, J. A. (2005) Subgraph centrality in complex networks. *Phys. Rev. E* **71**(5), 056103.
[32] Estrada, E., Sanchez-Lirola, M. G. & De La Peña, J. A. (2014) Hyperspherical embedding of graphs and networks in communicability spaces. *Discrete Appl. Math.* **176**, 53–77.
[33] Estrada, E., Vargas-Estrada, E. & Ando, H. (2015) Communicability angles reveal critical edges for network consensus dynamics. *Phys. Rev. E* **92**(5), 052809.
[34] Forman, R. (2003) Bochner's method for cell complexes and combinatorial ricci curvature. *Discrete Comput. Geom.* **29**(3), 323–374.
[35] Gao, L., Liu, X., Liu, Y., Wang, P., Deng, M., Zhu, Q., Li, H. (2019) Measuring road network topology vulnerability by ricci curvature. *Phys. A: Stat. Mech. Appl.* **527**, 121071.
[36] Ghosh, R., Lerman, K., Surachawala, T., Voevodski, K. & Teng, Sh (2024) Non-conservative diffusion and its application to social network analysis. *J. Complex Netw.* **12**(1), cnae006.

https://doi.org/10.1017/S0956792525000014 Published online by Cambridge University Press

[37] Gilson, M., Kouvaris, N. E., Deco, G. & Zamora-López, G. (2018) Framework based on communicability and flow to analyze complex network dynamics. *Phys. Rev. E* **97**(5), 052301.
[38] Gower, J. C. (1985) Properties of euclidean and non-euclidean distance matrices. *Linear Algebra Appl.* **67**, 81–97.
[39] Gromov, M. (1987) Hyperbolic groups. In *Essays in Group Theory*. Springer, 75–263.
[40] Higham, N. J. (2008) *Functions of Matrices: Theory and Computation*. SIAM.
[41] Jonckheere, E., Lohsoonthorn, P. & Ariaei, F. (2011) Scaled gromov four-point condition for network graph curvature computation. *Internet Math.* **7**(3), 137–177.
[42] Klein, D. J. & Randić, M. (1993) Resistance distance. *J. Math. Chem.* **12**(1), 81–95.
[43] Krislock, N. & Wolkowicz, H. (2012) Euclidean distance matrices and applications. In: Anjos, M. F. & Lasserre, J. B. (editors), *Handbook on Semidefinite, Conic and Polynomial Optimization*. International Series in Operations Research & Management Science, vol. 166. New York, NY, Springer.
[44] Lerman, K. & Ghosh, R. (2012) Network structure, topology, and dynamics in generalized models of synchronization. *Phys. Rev. E* **86**(2), 026108.
[45] Lin, Y. & Yau, Sh-T. (2010) Ricci curvature and eigenvalue estimate on locally finite graphs. *Math. Res. Lett.* **17**(2), 343–356.
[46] Markvorsen, S. (2008) Minimal webs in riemannian manifolds. *Geometr. Dedicata* **133**(1), 7–34.
[47] Najman, L. & Romon, P. (2017) *Modern Approaches to Discrete Curvature*. Cham, Switzerland, Springer, **2184**
[48] Narayan, O. & Saniee, I. (2011) Large-scale curvature of networks. *Phys. Rev. E* **84**(6), 066108.
[49] Ni, C.-C., Lin, Y.-Y., Gao, J., Gu, X. D. & Saucan, E. (2015) Ricci curvature of the internet topology. In 2015 IEEE Conference on Computer Communications (INFOCOM), IEEE. 2758–2766.
[50] Ollivier, Y. (2009) Ricci curvature of markov chains on metric spaces. *J. Funct. Anal.* **256**(3), 810–864.
[51] Pouryahya, M., Mathews, J. & Tannenbaum, A. (2017) Comparing three notions of discrete ricci curvature on biological networks, arXiv preprint arXiv: 1712.02943.
[52] Sandhu, R., Georgiou, T., Reznik, E., Zhu, L., Kolesov, I., Senbabaoglu, Y., Tannenbaum, A. (2015) Graph curvature for differentiating cancer networks. *Sci. Rep. UK* **5**(1), 12323.
[53] Saucan, E., Samal, A., Weber, M. & Jost, J. (2018) Discrete curvatures and network analysis. *MATCH Commun. Math. Comput. Chem.* **80**(3), 605–622.
[54] Skuhersky, M., Wu, T., Yemini, E., Nejatbakhsh, A., Boyden, E. & Tegmark, M. (2022) Toward a more accurate 3D atlas of C. elegans neurons. *BMC Bioinf.* **23**(1), 195.
[55] Sreejith, R. P., Mohanraj, K., Jost, J., Saucan, E. & Samal, A. (2016) Forman curvature for complex networks. *J. Stat. Mech. Theory Exp.* **2016**(6), 063206.
[56] Villani, C. (2009) Ricci curvature. *Optimal Transp. Old New* **338**, 357–420.
[57] Von Luxburg, U., Radl, A. & Hein, M. (2010) Getting lost in space: Large sample analysis of the commute distance. *Adv. Neur. Inf. Process. Syst.* **23**, 2622–2630.
[58] Weber, M., Stelzer, J., Saucan, E., Naitsat, A., Lohmann, G. & Jost, J. (2017) Curvature-based methods for brain network analysis, arXiv preprint arXiv: 1707.00180.
[59] White, J. G., Southgate, E., Thomson, J. N., Brenner, S., et al. (1986) The structure of the nervous system of the nematode caenorhabditis elegans. *Philos. Trans. R. Soc. Lond. B Biol. Sci.* **314**(1165), 1–340.
[60] Wu, Z., Menichetti, G., Rahmede, Ch & Bianconi, G. (2015) Emergent complex network geometry. *Sci. Rep. UK* **5**(1), 10073.

Cite this article: Estrada E. Forman–Ricci communicability curvature of graphs and networks. *European Journal of Applied Mathematics*, https://doi.org/10.1017/S0956792525000014